

The Axis Ratio Distribution of Local and Distant Galaxies. ¹

Stephen C. Odewahn ², David Burstein, and Rogier A. Windhorst

Dept. of Physics & Astronomy, Arizona State University, Box 871504, Tempe, AZ
85287-1504

Email: sco@poseidon.caltech.edu, raw@cosmos.la.asu.edu, burstein@samuri.la.asu.edu

Send preprint requests to “sco@poseidon.caltech.edu”

Date of this version: December 4, 2018

Received _____; accepted _____

¹Based on observations with the NASA/ESA *Hubble Space Telescope* obtained at the Space Telescope Science Institute, which is operated by AURA, Inc., under NASA Contract NAS 5-26555.

²Currently at Department of Astronomy, California Institute of Technology

ABSTRACT

Surface photometry from 16 HST/WFPC2 fields in the I_{814} -band filter is used to derive the distribution of apparent axis ratios for galaxies in progressively fainter magnitude intervals for $I_{814} \leq 25$. We assess the systematic and accidental errors in ellipticity measurements as a function of image resolution and signal-to-noise ratio, and statistically correct for the effect of cosmological surface brightness dimming on our isophotal measurements. The axis ratio distribution for the local galaxy population was computed using $\log R_{25}$ measurements for 1569 RC3 galaxies with $B_T \leq 13$ mag. Nonparametric tests are used to show that our distant samples, in the redshift range $0.1 \lesssim z \lesssim 1.0$ –1.5, are not statistically different from the local sample. We present image montages of galaxies selected randomly from different axis ratio and apparent magnitude ranges and discuss the evolutionary consequences of the lack of a strong difference between the ellipticity distributions in near and far data sets.

Subject headings: galaxies: elliptical — galaxies: spiral — galaxies: irregular — galaxies: evolution — galaxies: fundamental parameters

1. INTRODUCTION

The apparent isophotal axis ratio, b/a , of a galaxy is related to its intrinsic three-dimensional structure. A statistical recovery of the frequency distribution of intrinsic shapes using apparent axis ratios is dependent on the condition that galaxies are randomly oriented in space with respect to the observer. It is also dependent on the condition that known biases in the galaxy sample, such as those of Malmquist-type, or measurement systematics, and dust, etc., can be adequately modeled.

The first detailed study of the axial ratios of galaxies was made by Hubble (1926), who established the basic methodology used in later papers by de Vaucouleurs (1959), Sandage, Freeman & Stokes (1970), and de Vaucouleurs & Pence (1973). Subsequent work by Noerdlinger (1979) and Binney & de Vaucouleurs (1981) used mathematical inversion techniques to transform the observed $f(b/a)$ to the intrinsic distribution. Odewahn (1989) applied the modeling methods of the earlier papers to the much improved axis ratios and diameters that refer to a standard isophotal level in the RC3 (*cf.* de Vaucouleurs et al. 1991) to study intrinsic galaxy shapes as a function of morphological type. More extensive studies of this type, employing larger samples of photographic and CCD galaxy surface photometry are presented by Ferguson & Sandage (1989), Fasano & Vio (1991), Lambas et al. (1992), and Ryden & Terndrup (1994).

The principal aim of these papers was to determine the distribution of intrinsic shapes for galaxies drawn from different population samples, *e.g.*, from different morphological types or surface brightness classes. The intrinsic shape of the optical component of a galaxy is likely to be linked to the physical state of the dark matter halo and hence may present important information about the history and dynamical state of the system. Yet, any statistical approach to determine true axial ratios from observed ellipticities is valid only if two simplifying assumptions are made, and various systematic effects are taken into account.

These two simplifying assumptions are: a) that galaxies are randomly oriented in space with respect to the observer; and b) that all galaxies in a given sample have the same intrinsic three-dimensional form. Systematic effects include surface-brightness selection effects, Malmquist-bias types, sky subtraction errors, internal dust properties, and triaxiality of early-type (elliptical) galaxies. Hence, in practice it is very difficult to derive the 3-D shapes of galaxies. Lambas et al. (1992) find strong evidence for triaxiality among the early-type ellipticals, a situation which complicates the derivation of intrinsic shapes using the apparent axis ratio distribution. Our present purpose is *not* to derive the intrinsic shapes of galaxies as a function of Hubble type. Rather, we wish to use the observed ellipticity distribution as tool to search for evidence of dynamical galaxy evolution over a reasonably large fraction of the age of the Universe. We want to investigate if different galaxy populations with different ellipticity distributions (*i.e.*, disk- or bulge-dominated populations) are present at different flux levels (*i.e.*, different lookback times). In particular, we want to investigate if the epoch of the onset of disk formation can be delineated from the axis-ratio distribution of galaxies observed with the Hubble Space Telescope (HST).

Recently, Im et al. (1995) used the form of $f(b/a)$ to make inferences about the faint galaxy populations surveyed with HST. The $\sim 0''.1$ FWHM resolution provided by HST's Wide Field Planetary Camera 2 (WFPC2) allows the determination of the sub-kpc morphology and isophotal shapes of distant galaxies — as well as the population fractions of different galaxy types, over a wide range of epochs. The morphological properties of the faint galaxy population have recently been studied with HST by Driver et al. (1995a, 1995b, 1995b), Glazebrook et al. (1995), Cowie et al. (1995), Odewahn et al. (1996), and Abraham et al. (1996). These morphology-based studies found that a wider range of peculiar or disturbed morphologies are observed at faint magnitudes ($20 \lesssim I \lesssim 25$ mag, $0.5 \lesssim z \lesssim 1-2$), compared to what is seen in the local Universe. Uncertainties arising from cosmological effects such as bandpass shifting and $(1+z)^4$ surface brightness (SB) dimming complicate the interpretation of morphological classification systems for studying galaxy

evolution (Burg et al. 1997). The goal of the present study is therefore to compare the properties of nearby galaxies to those seen at high redshift with HST without regard to predicted Hubble type.

These tests using the galaxy axial ratio distributions are a useful counterpart to morphological studies to understand how galaxies at high z compare to those near us. Im et al. (1995) presented the axis ratio distributions for different HST galaxy types, as determined by bulge- and disk-decomposition of the HST images. This, however, assumes that the galaxy types can be determined reliably and independently from the axis ratios. It is not a priori clear that this can be done, and that the axis ratios therefore are independent of the galaxy type. Strictly speaking, we do not know which galaxy types seen at high redshift evolve into which kind of local counterparts in a universe if hierarchical clustering dominates, and therefore we prefer not to separate the axis ratios as function of galaxy type. Therefore, in this paper, we will compute the axial distributions for *all* galaxies detected on the deep HST images, irrespective of their predicted Hubble type. While we forego quantitative information of the axial ratio distributions of specific Hubble types, we benefit from inclusion of all galaxies, whether or not easily classified in a morphological type based on present-day galaxies (e.g., linear or “chain” galaxies).

In §2, we discuss the observations and their reduction using the automated image analysis system MORPHO. In §3, we discuss the systematic and accidental errors in axis ratio measurements in the regime of low resolution and/or low S/N ratio. We also discuss the errors that exist in the axial ratio distribution of the local galaxy sample from the RC3. In §4 we present our determination of the frequency distributions of apparent axis ratio in progressively fainter magnitude intervals. In §5 we discuss how our results can be related to existing morphological tests of galaxy evolution in terms of the hierarchical clustering/merger paradigm for the formation of galaxies.

2. OBSERVATIONS and REDUCTION

2.1. Observations

The HST data archive was accessed via STEIS to obtain a number of random WFPC2 fields with F814W images. The F814W filter was chosen to make a consistent measurement of axial ratios in the redshifted passband which — for $0.5 \lesssim z \lesssim 1.0$ — comes closest to the B passband for local galaxies. The deepest field analyzed in this work was the Hubble Deep Field (HDF; Williams et al. 1996), which for the present purposes has 49 exposures in F814W, yielding a 1σ surface brightness (SB) sensitivity of $I_{814} \leq 28 \text{ mag arcsec}^{-2}$, and a 5σ point-source sensitivity of $I_{814} \simeq 29.0 \text{ mag}$ (Odewahn et al. 1996).

A deep WFPC2 field surrounding the weak radio galaxy 53W002 at $z = 2.39$, was imaged in Cycles 4–5 using the F814W filter for 12 orbits (see *e.g.*, Driver et al. 1995a). These dithered images reach a 1σ SB sensitivity of $I_{814} \leq 26.7 \text{ mag arcsec}^{-2}$, and a 5σ point source sensitivity of $I_{814} \simeq 28.0 \text{ mag}$ (Windhorst et al. 1997). Moreover, the dark HST sky at 53W002’s location near the North Ecliptic Pole and the small galaxy scale-lengths (Odewahn et al. 1996) allow detection of compact galaxies in this field down to $I \lesssim 27 \text{ mag}$. Morphological studies of these images (hereafter referred to as the “W02” data set) are presented by Driver et al. (1995a) and Odewahn et al. (1996).

Two other sets of observations go less deep than HDF and W02: (1) the eight WFPC2 flanking fields surrounding the HDF (Williams et al. 1996) have mean integration times from 2500 sec to 5300 sec (hereafter referred to as the “HFF” data set). Six Medium Deep Survey Fields have mean integration times from 866 sec to 2100 sec (Driver, Windhorst, & Griffiths et al. 1995b; the “DWG” data set). Together, these 14 fields cover a sky area of 0.0168 deg^2 . Based on their total F814W galaxy number counts, we estimate that these shallower images have a 90% completeness limit of $I_{814} \lesssim 24.0 \text{ mag}$ for galaxies of average SB, although our use of these fields, listed in Table 1, will be restricted to the higher S/N images with total flux $I_{814} \lesssim 22 \text{ mag}$.

2.2. Data processing and catalog generation

Initial photometric catalogs of galaxies in each WFPC2 field were made using the SExtractor software (Bertin & Arnouts, 1996). This package is designed to locate discrete galaxy images and extract photometric parameters for extended sources in crowded galaxy fields. Candidates are defined to have at least 8 connected pixels with flux $\geq 2\sigma$ above the local median sky. In each case, a 3×3 gaussian smoothing filter is applied prior to detection. Adequate S/N is required to determine reliable isophotal axis ratios, so we cut our final catalogs well above the formal limiting magnitudes of each sample: *i.e.*, $I_{814} \leq 22.0$ mag for the HFF and DWG fields, $I_{814} \leq 25.0$ mag for the W02 field, and $I_{814} \leq 26.0$ mag for the HDF. Photometric zeropoints for each WFPC2 image were computed from the mean WFPC2 integration times and the synthetic zero points listed in Table 9 of Holtzmann et al. (1995).

Automated surface photometry of all cataloged objects was performed with the software package MORPHO (Odewahn 1995,1997; Odewahn et al. 1996), designed for neural network-based morphological classification of galaxies. The initial galaxy catalogs generated by SExtractor are used to cut postage stamp images around each detected galaxy. Local sky values are substituted for faint galaxy images close to each given object in terms of elliptical areas whose size, shape and orientation are established in a previous iteration by SExtractor. Local sky estimates are made by the MORPHO package by iteratively fitting a sloped plane to a surrounding empty sky-box (see Windhorst et al. 1991), excluding the area of all other objects found by SExtractor in that sky-box. We used for the first step an iterative rejection algorithm that determines the best local sky mode.

We compared the sky values from this automated surface photometry to those for ~ 50 faint objects in the *same* W02 images measured by Pascarelle et al. (1996) with a completely independent *interactive* package, that otherwise similarly used a sloped plane-fit to a surrounding visually empty sky-box. Both methods produce sky-estimates consistent within 0.07% (and consistent with Monte Carlo tests of the accuracy of this *interactive* sky

determination by Windhorst et al. 1991; W91). The two methods also give total aperture magnitudes mutually consistent within 0.05 mag, with $\text{rms} \simeq 0.22$ mag for each algorithm at the faint flux levels. Hence, we believe that our sky-errors are dominated by random (fitting) errors, but not by large-scale systematics.

We also compare the total magnitudes from the MORPHO (I_S) and SExtractor (I_M) packages for about 1200 galaxies. Using galaxies with $I_{814} \leq 22$, a mean zeropoint offset of $\langle I_S - I_M \rangle = -0.01$ was derived (negligibly small). A 3% scale error, significant at the 3σ level, was evident between the MORPHO and SExtractor magnitude systems. This result was anticipated since we compare the “Kron” magnitudes of SExtractor (magnitudes extrapolated to near-total using the second moment of the light distribution) to the isophotal magnitudes of MORPHO (integrated magnitude measured within an isophotal aperture sized to match a fiducial isophotal level). As expected, the SExtractor magnitudes are consistently brighter than the corresponding MORPHO values. For $I \leq 24$ mag, this systematic difference is described well by:

$$I_S - I_M = -0.01 - 0.035(I_S - 22) \quad (1)$$

We have adopted the MORPHO magnitudes for use in this paper, but give the following relation to bring the isophotal MORPHO magnitudes onto the total SExtractor system:

$$I_S = 0.966I_M + 0.73 \quad (2)$$

Over the range of magnitudes to be investigated here, $19 < I_{814} < 25$, this systematic difference will result in a change of at most 0.25 magnitudes, or 12% of the width of the binning interval used in this work to divide our galaxy samples.

Surface photometry is performed on each of the patched postage stamp images using the MORPHO image analysis package. This provides ellipse fits over a range of isophotal

levels (based on the local sky-noise) and elliptically averaged surface brightness profiles, as well as sets of photometric parameters known to show significant dependence with morphological type for more nearby galaxies as well as HST galaxies (Odewahn & Aldering 1995, Odewahn et al. 1996).

As discussed in §4, we expect that a significant portion of our faint galaxy sample ($I \gtrsim 24$) will have redshifts of $z \gtrsim 0.5$, and hence will suffer significant cosmological SB dimming. For this reason, an ellipse fitting package was added to MORPHO that uses axis ratio measurements over a range of isophotal levels and that uses an estimate of the redshift, z , based on the expected median redshift vs. I_{814} magnitude relation. For this, we used the measured redshift-magnitude relation from Lilly et al. (1995) for $I \leq 22$ mag, and photometric redshift estimates by Sawicki et al. (1996) for $I \leq 25$ mag, to estimate the proper *restframe* surface brightness level for measuring the apparent axis ratio b/a .

We cleaned our final galaxy sample using an interactive MORPHO package which plots mosaics of the selected galaxy postage stamps with the isophotal ellipse fits overplotted. In some cases, image merging due to nearby galaxies or diffraction spikes from nearby stars made it impossible to compute reasonable ellipse fits. Such cases, comprising less than 5% of the cataloged images, were interactively rejected from subsequent analysis. These rejected galaxies were isolated and their $f(b/a)$ distribution was compared to that of the bonafide galaxy sample to assure that no strong signature in the apparent axis ratio distribution was being removed.

3. SYSTEMATIC ERRORS IN AXIS RATIO MEASUREMENTS

Given the fundamental differences between the HST images and those from different ground-based telescopes, it is inevitable that systematic errors will exist for any comparison of axial ratios of galaxies observed with these instruments. As a result, we should expect that comparisons between photometric properties of local and high redshift galaxies will

likewise suffer from systematic measurement errors. We note that such errors occur at both low redshift and at high redshifts. For example, even with the superb resolution of HST, images of high redshift galaxies ($z \gtrsim 1$) suffer from poor linear resolution and low S/N. As we go fainter with the HST images, our ability to measure meaningful isophotal parameters such as size and shape becomes progressively impaired. Separately, existing axial ratio data for nearby galaxies suffer either from being a mix of direct measurements from images and eye estimates (such as in the RC3), and/or from problems of zero point calibration and sky subtraction issues (e.g., purely CCD-based surveys).

We adopt the point of view that there is no one “correct” measurement of the axial ratios of galaxies, but rather a series of different kinds of measurements that need to be brought onto the same internal system. As such, it is imperative to understand how our apparent axis ratio measures are affected by these systematics as we progress to fainter magnitude intervals. Similarly, we need to test how consistent are our ellipticity data for nearby galaxies.

3.1. Image Simulations of the Distant Galaxy Sample

The MORPHO program allows us to simulate the appearance of a galaxy of known redshift at some user-specified higher redshift. This package is designed primarily to simulate the effects of cosmological SB dimming at high redshift predicted by the equations given in Weedman (1986), with K-corrections of Lilly et al. (1995). With the $\Theta - z$ relation used by Bohlin et al. (1991), Hill et al. (1992), and Mutz et al. (1994) for $H_0 = 75$ km/s/Mpc and $q_0 = 0.5$, images of local galaxies with high resolution and S/N were repixelated to yield the resolution that would have been observed at redshift z with the WFPC2 pixel size of $0''.0996$. Sets of high redshift images were simulated using two sets of input images: (1) 63 B_J images of local galaxies ($z \leq 0.05$) from the Frei et al. (1996) sample, and (2) a subset of 223 galaxies observed with WFPC2 in I_{814} with $I \leq 22$ mag from Driver et al. (1995a, 1995b). In both cases, we want to simulate the appearance of galaxies observed at high

redshift ($z \gtrsim 0.5$) in the I_{814} bandpass with WFPC2.

For the B_J galaxy sample of Frei et al. (1996) with $B_T \leq 13$ mag, we assume a mean redshift of $\langle z \rangle = 0.007$, based on the mean of 1569 galaxies with measured V_{gsr} km/s (redshift relative to the galactic standard of rest) in the RC3 for $B_T \leq 13$ mag. The Frei sample was used to get a rest-frame bandpass as close as possible to that of our HST I_{814} observations of high redshift galaxies, therefore accounting for the K-correction to first order. We note that B_J , centered at 4500\AA , may strictly only be used to simulate the I_{814} -band appearance of galaxies in the range $0.6 \lesssim z \lesssim 1$, and that higher redshift modeling will require the use of large samples of U images. However, as noted by Odewahn et al. (1996), the systematic changes across the U_{300} , B_{450} , V_{606} , and I_{814} filters in effective radius and isophotal axis ratio are small (less than 15%) for galaxies in the HDF and 53W002 fields (see also figure 1 of Burg et al. 1997). Hence, we used the Frei B_J images to simulate galaxy images to $z \leq 1.6$, where the HST I_{814} filter samples around rest-frame 3000\AA . On the basis of z measurements from the CFRS (Lilly et al. 1995) and the photometric redshift estimates in the HDF (Sawicki et al. 1997), we adopt a median redshift for our sample of 223 I_{814} galaxy images with $I_{814} \leq 22$ mag of $z_{med} \lesssim 0.5$. The B_{450} and V_{606} images of these lower redshift galaxies are used to simulate the appearance of more distant galaxies ($z \lesssim 1.2$) observed in I_{814} .

Each of the 63 Frei B_J galaxy images is used to simulate galaxies at redshifts of $z = 0.3, 0.6, 0.9$, and 1.6 . Each of the 223 galaxies in the bright I_{814} sample ($z \lesssim 0.5$) is used to simulate galaxies at redshifts of $z = 0.6, 0.8$, and 1.2 . These simulated images are reduced with exactly the same MORPHO routines as used in § 2 for our actual WFPC2 images. These simulated measurements are then used to study the change in measured axis ratio as a function of S/N ratio and linear resolution for every type of galaxy, using their known “true” b/a from the high resolution and high S/N ground-based images. The S/N ratio of the galaxy image in the distant galaxy simulation is computed using the integrated signal within an optimally selected elliptical aperture (measured at an approximate surface

brightness of $\mu_I = 24.5 \text{ mag arcsec}^{-2}$) and the standard deviation of the local sky, whose mode was determined after a few iterations of outlier rejection. As a measure of image resolution, R , we use the number of pixel elements along the major axis of this optimal isophotal ellipse. Axis ratio changes are measured with residuals computed as $(b/a)_o - (b/a)_z$, where $(b/a)_o$ is the isophotal shape measured in the original local galaxy image, and $(b/a)_z$ is the value measured in the simulated high redshift image. For subsets of $(b/a)_o$, we search for systematic trends with S/N and resolution to assure that the local comparison set is as much as possible bias-free.

The results of the I_{814} image experiments for galaxies with $(b/a)_o \leq 0.5$ are summarized in Figure 1. Two major points are clear from these diagrams: (1) b/a measurements are dominated by accidental errors, as evidenced by the large scatter in both panels of Figure 1, and (2) images with intrinsically small axis ratios are measured systematically more round (large b/a) as the resolution and/or S/N are decreased. In Figure 1, we plot for 176 simulated high z galaxy images a linear least squares regression line fit for $(b/a)_o - (b/a)_z$ vs. $\log(\text{S/N})$. Although dominated by a large scatter, the measured slope of $\alpha = 0.049 \pm 0.014$ is statistically significant at the 3.5σ level, and predicts residuals in the sense expected: faint, low S/N images are measured to be systematically too round.

In Fig. 1b we show the same fit relative to $\log(R)$ with a fitted regression of slope $\alpha = 0.067 \pm 0.019$, again significant at the 3.5σ level, and with again the same effect: faint compact images tend to be measured too round. The residual axis intercepts of these fits predict offsets of $(b/a)_o - (b/a)_z = 0.05$ at $\text{S/N} = 100$ and $R = 32$ respectively. Similar fits using image simulations of galaxies with $(b/a)_o \geq 0.5$ showed no statistically significant trends with S/N and R . *Summarizing both results, intrinsically round galaxies at high redshift are not measured to be systematically too flat, but intrinsically flat galaxies are measured too round.* Results obtained with image simulations using the Frei B_J galaxies were consistent with our I_{814} -band experiment. The measured slopes had the same magnitude and sense as for I_{814} simulations. These results were significant at only the 2σ

level due to a smaller number of input galaxies with $(b/a)_o \leq 0.5$ (only 18 such cases).

As expected, S/N and R are highly correlated (correlation coefficient of 0.86), and hence it is difficult to determine if one image property really dominates the effect observed in Figure 1. Independent of this, the important result of these experiments is that we can now predict systematic b/a measurement errors on the basis of easily *measured* properties of images. The bulk of the errors resulting from this effect are accidental, but important systematic trends are derived from the data in Figure 1 of the form:

$$(b/a)_o - (b/a)_z = 0.067 \log R - 0.151 \quad (3)$$

or

$$(b/a)_o - (b/a)_z = 0.049 \log S/N - 0.148 \quad (4)$$

Although relatively small, we must consider this systematic effect in §4 when we compare local galaxies (observed with high resolution and large S/N) and high redshift galaxies (poor resolution and low S/N).

3.2. Consistency of Near and Distant Galaxy Samples

Since we have chosen galaxies at high redshift on the basis of their apparent magnitudes in I_{814} , we must choose present-day galaxies by the same criterion in the de-redshifted filter for the expected redshifts of our distant galaxies. As such, we choose a bright subset of the B-band data ($B_T \leq 13.0$ mag) contained in the RC3 for our local sample of galaxies with measured axial ratios. For each galaxy, the RC3 gives the decimal logarithm of the isophotal axis ratio, $R_{25} = (D/d)_{25}$, where D and d are the major and minor axis lengths measured at 25.0 mag arcsec⁻² in the B_{450} (note that the RC3 defines D_{25} in units of 0.1 arcmin). As discussed by de Vaucouleurs et al. (1991), the majority of these axis ratios

are based on visual estimates from a variety of sources, but have been transformed to a self-consistent system via comparisons with detailed surface photometry for a sample of 608 galaxies. For galaxies fainter than $B_T \gtrsim 13$ mag — the nominal limit of the original Shapley–Ames (1932) Catalog — the RC3 galaxies represent a heterogeneous sample which suffers from a variety of selection effects.

The 1569 galaxies in the RC3 with $B_T \leq 13.0$ mag have other parameters in the range: $0.0 \leq \log R_{25} \leq 1.2$, $\log D_{25} \geq 0.5$, and $-7 \leq T \leq 10.0$, where T is the morphological Type in the revised Hubble system. This galaxy sample is essentially a somewhat enlarged version of the original Shapely-Ames Catalog, and should be reasonably complete to $B_T \leq 13.0$ mag except for dwarf or extremely low surface brightness galaxies.

To test the consistency of the RC3 eyeball axis ratios with our own MORPHO machine measurements of axis ratios, we compare the MORPHO measurements to the RC3 measurements for 145 galaxies: 63 galaxies observed in B_J by Frei et al. (1996) and 82 UGC galaxies observed in B by de Jong (1994) using CCD images. The automated surface photometry package in MORPHO was used to estimate isophotal axis ratios for these 145 galaxies at $\mu_B = 25$ mag arcsec⁻². The resulting difference, $b/a(\text{RC3}) - b/a(\text{MORPHO})$ is plotted versus $b/a(\text{RC3})$ in Figure 2. A linear least squares fit to only the 63 galaxies of the Frei et al. data gives a slope of 0.21 ± 0.01 and an rms scatter 0.07. The deJong sample does not cover a wide range of b/a (the galaxies were selected to have $b/a \geq 0.6$), but their values of $b/a(\text{RC3}) - b/a(\text{MORPHO})$ are consistent with those of Frei et al. in the region where their ellipticities overlap. Hence, it appears that the eyeball RC3 b/a estimates are systematically flatter for flat objects, and systematically rounder for round objects.

The origin of this small, but statistically significant trend is unknown at present, but obviously important for the comparison with HST data. Based on this fit we adopt the following correction formula to transform the 1569 RC3 axis ratios to our own MORPHO measurements, so that now for both the low and the high redshift galaxies we can measure a consistent ellipticity by machine:

$$(b/a)_c = 0.80(b/a)_{RC3} + 0.12 \quad (5)$$

Given the uncertain reason for making such a correction, we will in §4 examine how both the original RC3 axial ratio distribution and the axial ratio distribution for our 1569 local galaxy sample — when transformed to the MORPHO system — compare to those of high-redshift galaxies.

It is important to note that the linear correction implied by equation 5 is used for convenience, as the present data in this comparison are too few to derive a formally correct relationship. The reader will note that a correction of this form will deplete the nearly circular apparent axis ratios ($b/a \geq 0.92$), as well as predict unrealistically elongated galaxies. This clearly would complicate the derivation of the 3-D axial ratio on the basis of $f(b/a)$ (not our purpose here), especially in light of the triaxiality question for early-type systems (Lambas et al. 1992). A nonlinear expression is required for such a correction, however the lack of highly elongated and circular isophotal shapes in our present sample overlapping the RC3 is too small for such a derivation. Since the statistical tests discussed in §4.2 are most sensitive to changes at more intermediate axis ratios, particularly around the median, we feel justified in making this correction for the purposes of comparing low and high redshift samples.

4. APPARENT AXIS RATIO DISTRIBUTIONS - NEAR AND FAR

4.1. Subdividing the Distant Sample

The 16 WFPC2 fields listed in Table 1 were processed with MORPHO to assemble photometric catalogs to the depths given in §2 on the basis of total integration time. Using the I_{814} -band vs. z data of Lilly et al. (1995) for $I_{814} \leq 22$ and the photometric redshift estimates of Sawicki et al. (1997) for $I_{814} \leq 25$, we specified a series of magnitude intervals for drawing galaxy samples with progressively higher median redshift and adequate

statistical size. Unlike the local galaxy samples, fitting isophotal shapes at a fixed SB level is inadequate. Due to cosmological effects, the change in observed SB is $\Delta_\mu = 10 \log(1+z)$ mag arcsec⁻². Hence, fitting ellipses at a fixed isophotal level in a high redshift galaxy gives a measurement of isophotal shape in an intrinsically brighter region of the galaxy. In the case of an early-type, bulge-dominated system where the higher surface brightness isophotes often have rounder shapes than the lower surface brightness outer disk isophotes, we may expect to see a trend in b/a with surface brightness. The same, or in fact the opposite, may be true for the faint Irr galaxies that dominate the HST images, as we will address in the simulations below.

In order to avoid possible systematic errors in our current analysis, we ran MORPHO in a mode where multiple ellipse fits are made at progressively fainter surface brightness levels. These levels are chosen on the basis of S/N in the local sky-background. For each galaxy, we used the apparent total I_{814} magnitude to estimate a median z for the corresponding magnitude bin. The cosmological correction to SB, Δ_μ , is then applied to the desired isophotal level (25.0 mag arcsec⁻² in B_{450} was adopted here), and an interpolated value of the axis ratio at the correct intrinsic surface brightness is computed. While not a perfect way to compensate for redshift effects, it is the best we can do until all the galaxies sampled have individual redshifts measured for $I_{814} \lesssim 26$ mag, which is a major challenge even for 8–10 meter telescopes. The final WFPC2 samples consists of:

1. a bright sample of 105 galaxies in the range $I_{814} \leq 20$ mag with $\langle I_{814} \rangle = 19.9$ mag at an estimated median redshift of $z \approx 0.2$ and a mean SB threshold of $\mu_I = 23.9$ mag arcsec⁻² ;
2. 254 galaxies in the range $20 \leq I_{814} \leq 22$ mag with $\langle I_{814} \rangle = 21.3$ mag at an estimated median redshift of $z \approx 0.5$ and a mean SB threshold of $\mu_I = 24.6$ mag arcsec⁻² ;
3. 210 galaxies in the range $22 \leq I_{814} \leq 24$ mag with $\langle I_{814} \rangle = 22.8$ mag at an estimated median redshift of $z \approx 0.8$ and a mean SB threshold of $\mu_I = 25.5$ mag arcsec⁻² ; and

4. a faint sample of 296 galaxies in the range $23 \leq I_{814} \leq 25$ mag with $\langle I_{814} \rangle = 24.2$ mag at an estimated median redshift of $z \approx 1.0$ and a mean SB threshold of $\mu_I = 26.0$ mag arcsec $^{-2}$.

The differential frequency distribution of apparent axis ratios for each magnitude selected sample was computed using fixed bins of 0.05 in b/a . The results are plotted in Figures 3 through 5, where the WFPC2 samples are represented as open circles connected by thin dotted lines.

4.2. Comparing RC3 and Distant Samples

In accounting for systematic errors in both the distant and nearby galaxy samples, we have chosen to model how RC3 galaxies would appear at the median redshift for each distant galaxy sample, including measured S/N and linear resolution effects (§3.1). Various methods are used to simulate the corresponding $f(b/a)$ distribution we expect to observe for the RC3 sample at a given median redshift *if* the galaxy population mix at that epoch were the same as our local RC3 sample. The apparent magnitude of a galaxy in the RC3 sample is estimated for $H_0 = 75$ km/sec/Mpc and $q_0 = 0.5$ using:

$$m - M = 42.38 - 5 \log h_0 + 5 \log z + 1.086(1 - q_0)z + \Delta m_K + \Delta m_L \quad (6)$$

where $\log h_0 = H_0 / 100$, and M is the absolute magnitude of the galaxy computed using B_T and V_{GSR} (from RC3). Type dependent K-corrections, Δm_K , were computed from Figure 1 of Lilly et al. (1995) and applied to the distance modulus of equation 6. Driver et al. (1995) and Lilly et al. (1995), respectively, note that there is substantial evidence of strong luminosity evolution since $z \gtrsim 0.5$ for late-type galaxies ($T \gtrsim \text{Sc}$) and blue galaxies, respectively. The morphological number counts in B_{450} by Odewahn et al. (1996) also show that smaller levels of luminosity (and/or density) evolution have occurred in B_J for E+S0 and early-type spiral populations for $z \lesssim 1$.

To account for these possible evolutionary effects on our apparent magnitude estimates for the redshifted RC3 galaxies, we applied a redshift-dependent apparent magnitude increase, Δm_L , for E+S0, Sabc and Sd/Irr galaxies following the models of Driver et al. (1995b): $\Delta m_L = 0$ for all galaxies with $z < 0.2$; $\Delta m_L = -0.5, -1.0, -1.5$ respectively for E+S0, Sabc and Sd/Irr galaxies with $0.2 \leq z \leq 0.75$; and $\Delta m_L = -1.0, -1.5, -2.5$ respectively for E+S0, Sabc and Sd/Irr galaxies with $z > 0.75$. These estimates are used only to investigate the possible effects of luminosity (and/or implied density) evolution on our predicted $f(b/a)$ for galaxies out to $z \lesssim 1.2$, and we do not suggest that these are necessarily the exact amounts of luminosity evolution for each of these galaxy classes.

On the basis of the apparent magnitude computed in this manner, each redshifted RC3 galaxy was binned by apparent magnitude. The resulting magnitude-binned sets of b/a were used to compute the observed $f(b/a)$ distributions for a local (*i.e.*, RC3-like) population seen at high redshift. Each RC3 b/a estimate was corrected to the MORPHO system using Equation 5. These predicted distributions are plotted as solid squares connected by bold solid lines in Figure 3. On the basis of Figure 3, one might infer a depletion of highly flattened axis ratios ($b/a \lesssim 0.4$) at progressively higher redshifts ($I \gtrsim 22$ mag or $z \gtrsim 0.4$) compared to our local population.

We have used two methods to compare the WFPC2 b/a distributions with those from the “redshifted” RC3 data sets. A Kolmogorov-Smirnoff probability, $P(KS)$, was computed for each set of distributions to assess the likelihood that the two distributions were drawn from the same parent population. The $P(KS)$ statistic gives the probability that the largest deviation between the two cumulative distributions drawn from each data set is due to random fluctuation, and hence a small value of $P(KS)$ would indicate that the difference between two data sets is statistically significant. We have used the conservative level of $P(KS) \leq 0.01$ to confirm that two sets are drawn from a different parent distribution. Values of $P(KS)$ are tabulated in each b/a set compared in the panels of Figures 3 through 5. For the brightest and faintest magnitude ranges, the $P(KS)$ probability just fails to

confirm that $f(b/a)$ for the WFPC2 samples is different from that of the RC3 set. The two intermediate ranges, covering $20 \leq I_{814} \leq 24$, confirm to better than a 99.9% confidence level that the two distributions are drawn from different parent populations. As noted by Press et al. (1986), the KS test has the advantage that it is a nonparametric test that is independent of data binning, but since all cumulative distributions are the same at the low and high ends, it is sensitive primarily to changes in the central region of the distribution around the median. We are primarily concerned with comparing the low axis ratio end of our high and low redshift samples, and hence use a second simple statistic for this case. For each b/a set, we compute the ratio, $\phi(b/a)$, of the number of galaxies with axis ratio smaller than b/a to the number of galaxies with axis ratio larger than b/a . Larger values of $\phi_i(b/a)$ indicate a higher fraction of flat cases (low b/a). To compare each set of distributions, we compute the difference between these values, $FD = \phi_{RC3}(0.4) - \phi_{WFPC2}(0.4)$, to form an index that measures the relative enhancement or depletion of flat systems at high redshifts. When FD is large and positive then the WFPC2 samples must be relatively poor in flat cases relative to RC3. The value of FD for each distribution comparison is also plotted in the panels of Figures 3 through 5. In Figure 3, this simple statistic confirms our KS test results in the sense that we do find FD to be different and progressively larger in the faint magnitude samples.

To see a more realistic distribution of axial ratios predicted for the RC3 at high redshift, we have to take into account systematic measurement effects due to degradation of S/N and linear resolution with redshift, specifically the results of equation 3 and equation 4 (§3.1). To do this, the apparent I_{814} magnitude estimated for each RC3 galaxy was used to estimate the expected R and S/N that would have been obtained had the galaxy been observed with an integration time appropriate to a given data set (*i.e.*, HFF, HDF, etc...). We then applied equations 3 and 4 to the redshifted RC3 distributions based on these values of R and S/N.

Equations 3 and 4 correct the observed b/a values as a function of $\log R$ and S/N ,

with the highest corrections coming for the most-edge on galaxies. In the present case, this means that the most edge-on galaxies in the RC3 seen today will have their axial ratios measured rounder with decreasing values of S/N and R . However, within the errors of the calculations presented in §3.1, we were unable to detect a strong systematic change in measured b/a for galaxies with intrinsic $b/a \gtrsim 0.5$. In order to avoid a discontinuous jump in the b/a properties of our corrected high redshift samples, we have applied a smoothing factor to the correction predicted by equation 3: the full correction is applied for $b/a \gtrsim 0.45$ with the correction decreasing to 10% of that predicted by equation 3 at $b/a = 0.8$. The basic properties of the predicted high redshift $f(b/a)$ distribution were found to be rather insensitive to the form of this smoothing function. The systematic b/a changes estimated in this way were applied to all measurements composing the “redshifted RC3” catalog.

The bold-line $f(b/a)$ distributions in Figures 4 are derived from these “resolution-corrected” redshifted RC3 samples. It should be noted that we applied R and S/N corrections independently, and found the results to be unchanged. For simplicity, we show only the R corrected estimates in our $f(b/a)$ plots. The important point to be noted in Figure 4 is that our apparent dearth of flattened systems at high redshift ($I \gtrsim 22$ mag or $z \gtrsim 0.4$, see Figure 3) has generally disappeared after applying these corrections. With the exception of the $20 \leq I_{814} \leq 22$ interval, the $P(KS)$ probability indicates no significant difference between the sets of low and high redshift distributions. The large jump in FD that was observed in the high redshift samples in Figures 3, which indicated a 19% increase in the relative fraction of flattened systems at low redshift, has now dropped to the $\lesssim 5\%$ level.

Not only do the S/N and R corrections remove many edge-on galaxies from the high redshift samples, the correction to make the eyeball RC3 axial ratio distribution consistent with the MORPHO machine measurements does so as well. If we had made this study comparing just the local RC3 axial ratio distribution (uncorrected) to that of the distant galaxy samples (uncorrected), we would have found a very large difference in the numbers

of edge-on galaxies seen today versus those seen at high redshift, with possibly erroneous conclusions about morphological evolution of galaxies as a consequence. However, to do so would be not correct in our opinion. Rather, by correcting for detectable systematic effects, we find the present-day axial ratio distributions of galaxies — when moved out to high redshift and accounting for all possible systematics as well as we can — to be very similar to those for HST galaxies with $0.3 \lesssim z \lesssim 1.0$.

To what extent is the lack of detection of a change in ellipticity in the range $0.3 \lesssim z \lesssim 1.0$ consistent with what we currently know about the morphologies of galaxies at these redshifts? As discussed in Driver et al. (1995), Odewahn et al. (1996), and Abraham et al. (1996), the galaxy population appears to be increasingly dominated by late-type (types later than Sc) at high redshift ($I \gtrsim 21$ mag, $z \gtrsim 0.5$). The $f(b/a)$ distribution for E+S0 and early spiral populations are different among the *local* galaxies (Binney & de Vaucouleurs 1980; Lambas et al. 1992). The E+S0 $f(b/a)$ show a smooth increase in the frequency of galaxies with increasing b/a , while the spirals show a rather flat distribution with a sharp drop in frequency around $b/a \approx 0.3$. For the very latest types (later than Sd), the $f(b/a)$ distributions computed in Odewahn (1989) are even more strikingly different from the early- and mid-spiral samples, with a pronounced redistribution of objects at the high (=round) b/a end of the distribution. Hence, a population dominated by late-type spiral systems at high redshifts could produce a relative overabundance of round objects in $f(b/a)$ with $b/a \gtrsim 0.6$.

As a test of this possibility, we altered the input catalog of RC3 galaxies to reflect a population that is dominated by a late-type spiral and irregular galaxies, as in the deep HST images of Driver et al. (1995a) and Odewahn et al. (1996). For our original sample of 1569 RC3 galaxies with $B_T \leq 13$, the type fractional percentages are $f(\text{E+S0}, \text{Sabc}, \text{Sd+Irr}) = (32\%, 48\%, 20\%)$, respectively. We randomly sampled this catalog to readjust these values to $f(\text{E+S0}, \text{Sabc}, \text{Sd+Irr}) = 10\%, 30\%, \text{ and } 60\%$, to create a sample more in line with the population fractions implied by the faint WFPC2 morphological studies mentioned

above. This spiral/Irr-rich “local” catalog was shifted to the same high redshift intervals used in Figures 3 (with systematic corrections as in Figure 4), and is shown in Figure 5. As is evident from comparing Fig. 4 to Fig. 5, we see only small changes in the predicted $f(b/a)$ functions when compared to the original local RC3 type fractions. The tendency to produce a more peaked distribution at the high b/a end is only mildly apparent, and this happens only in the high redshift bins where the observed late-type fraction is increased due to strong luminosity evolution in the late types (see Driver et al. 1995a) and to the loss of early-type galaxies from the redshifted local samples due to their larger K-corrections. Hence, it would seem that only an unreasonably extreme alteration of the type fractions (beyond those allowed by the studies of Driver et al. 1995 and Odewahn et al. 1996) would produce a detectable change in our currently observed WFPC2 samples.

Finally, we think that seeing is believing. Hence, we have put together montages of galaxies (Figures 6– 8) with similar ranges in b/a including: representative Frei et al. (1996) galaxies seen today in the B passband; the same Frei et al. galaxies placed at $z \sim 0.6$; and representative galaxies from our WFPC2 images, spanning a range of $I_{814} = 14$ to 25 mag. As one can see, there is little difference in morphology within each range of b/a . These figures illustrate that our use of B-band images for present day galaxies and I_{814} images for distant galaxies can produce systematic effects that are not quantifiable with the present data sets. In particular, it should be noted that the appearance of the galaxies becomes more asymmetric in the fainter magnitude intervals. This is most evident in the low b/a montage of Figure 6. Whether such changes are due to genuine morphological variation, or some cosmological effect is still open to question. As discussed in Bohlin et al. (1991), Giavalisco et al. (1996) and Odewahn et al. (1996), the appearance of some types of galaxies can change substantially as a given passband effectively samples bluer or rest-frame UV emission at higher redshift. Even though we have used the I_{814} -filter for our HST data to get a better match to the rest-frame B-band observations for our local sample, this match is not perfect. In the future, we will also make a comparison with a U-band survey in progress of a large number of UGC and NGC galaxies with the VATT telescope (see Burg

et al. 1997).

5. DISCUSSION

5.1. Comparison to other HST findings

Morphological type fractions have been shown to change systematically at fainter magnitudes or at higher redshift. The rather drastic increase in late-type systems at $z \gtrsim 0.5$ observed by Driver et al. (1995), Glazebrook et al. (1995), and Odewahn (1996) is interpreted as evolution among the galaxy populations at high redshift. From numerous papers referenced in our introduction, it is well known that early- and late-type systems display different apparent axis ratio distributions locally, and hence it was surprising that a large change in the fraction of Sd/Irr galaxies at high redshift would not manifest itself strongly in the observed axis ratio distributions. On the contrary, as we have shown in the previous section, only small deviations in the $f(b/a)$ distribution for high redshift galaxy samples are present compared with local samples. In fact, these small deviations may be totally explained if we take into account systematic errors in isophotal parameters measured in images with low linear resolution and low signal to noise. The observed $f(b/a)$ distribution for faint galaxy samples will also be affected by two additional factors: weak lensing and the possible influence of a population of linear "chain galaxies" at high redshift.

The shapes and orientations of distant galaxy images will be distorted from gravitational lensing by intervening mass distributions. Tyson et al. (1990) and Kaiser and Squires (1993) have used this effect to probe the mass distributions in rich clusters in an effort to confirm mass determinations derived from purely dynamical methods. The samples used in our current study were drawn from a variety of positions on the sky and are not expected to be profoundly influenced by foreground rich clusters. The presence of rich clusters in our current samples would manifest themselves by increased number counts relative to the field. On the contrary, the (morphological) number counts derived from the samples used

here were found by Driver et al. (1995) and Odewahn et al. (1996) to be very consistent.

However, the weak distortion of faint galaxy images caused by lensing from large scale structures (LSS) in the Universe must be considered. Large scale deviations in the mass distribution inferred from systematic galaxy redshift surveys by Huchra et al. (1988) and the measurement of fluctuations in the cosmic microwave background by COBE (Smoot et al. 1992) indicate that large matter overdensities may be common throughout the Universe, and that lensing resulting from these inhomogeneities may produce ellipticity changes of up to 3% for galaxies as distant as $z \approx 1$. A recent measurement of this weak distortion by LSS is presented by Mould et al. (1994), in a ground-based study of 4363 galaxies to a limit of $r \approx 26$ mag. They find a weak lensing signal significant at the 1σ level in the form of a mean position angle polarization of 1% over that expected for a random distribution. The detection of galaxy-galaxy lensing has been studied by Tyson et al. (1985) in a sample of 47000 galaxy images in the range $22.5 \leq B_J \leq 23.5$ with no statistically significant signal above that expected for a purely random distribution. More recent CCD-based studies by Brainerd et al. (1996) use 3202 galaxy pairs in the range $23 \leq r \leq 24$ mag to detect a lensing signal in the form of a position angle polarization of $1.1\% \pm 0.6\%$. They report that an ellipticity of approximately 2-3%, similar to the observed polarization effect, will be induced in faint galaxy images with angular separations of $\theta \approx 3''$ from bright galaxies. In the course of this ground-based study, they considered the ellipticity distribution of galaxies from their faint samples, and determine that the ellipticity distributions of these objects are consistent with $f(b/a)$ drawn from brighter, more local samples. Finally, the presence of a large amount of image distortion by LSS should be accompanied by a large amount of multiple imaging, an effect which is not observed commonly in well-studied distant radio galaxy samples (Blandford, private communication). The overall conclusion from these studies is that weak gravitationally lensing may certainly influence the observed $f(b/a)$ of faint galaxies by “stretching” the isophotal image contours. However, recent redshift surveys by Lilly et al. (1995) and Ellis et al. (1996) suggest that the median redshift of the galaxy sample used here is $z \lesssim 1$, and thus the overall image distortions due to lensing will

produce a rather small 1-2% systematic effect.

Separately, a population of faint blue galaxies with very narrow shapes and lumpy morphologies was reported by Cowie et al. (1996) and termed “chain” galaxies, a possibly new morphological class of galaxy common during younger epochs of the Universe. A truly linear structure, such as the chain galaxies are thought to be, will present an isophotal shape having a small value of b/a in nearly any spatial orientation. Hence, the presence of a large population of such galaxies in our faint samples could skew our observed $f(b/a)$ towards the low b/a end. The presence of such a new morphological population has been refuted by Dalcanton and Sheckman (1996), who claim that these galaxies do indeed exist at low redshift and represent edge-on views of low surface brightness late-type ($T \gtrsim \text{Sd}$) disk galaxies. Using a low-redshift sample of low surface brightness galaxies (central disk surface brightness $\mu \geq 21.3 \text{ mag arcsec}^{-2}$ in the r band), Dalcanton & Sheckman show that the $f(b/a)$ of this chain galaxy sample is consistent with that of a population of thin disk galaxies viewed with random orientations. The galaxies with the the smallest b/a display morphological similarities with the “chain” galaxies, especially in the far- UV .

The UIT images by O’Connell et al. (1997) and Marcum et al. (1997) of ordinary nearby disk galaxies seen edge-on resemble those of high redshift “chain galaxies”, so that the clumpy rest-frame UV -morphology of such objects at high redshift may be classified as a different or new class of object, while in reality they may not be. Our observations are consistent with this latter view. However, Pascarelle et al. (1996) note that the Cowie et al. (1996) chain galaxies are a clear minority of the faint blue galaxy population in deep WFPC2 images. The faint chain galaxies often do show clear “dumbbell” structure with most of the light in clumps at both outer ends — unlike many of the UIT images of nearby edge-on galaxies — so that these objects might be subgalactic sized clumps seen directly after or during their first mergers, which would trigger subsequent starbursts and form disks from gaseous material that settles into rotation during and after the merger. Hence, they could be short-lived “chain-like” objects, but their fraction of the total population is

not large enough to significantly affect our b/a distributions.

5.2. Comparison to the Hierarchical Clustering/Merging Galaxy Formation Scenario

Consider what we might expect to see at high redshift from galaxies that form via the hierarchical cluster/merger hypothesis (e.g. Gott & Rees 1975). Peebles (1993) defines lookback time to be the time measured backwards from the present time, in other words, since $z = 0$. Hence, larger values of lookback time correspond to earlier cosmic epochs (and larger redshift) in the Universe. The familiar galaxy types we see today are thought to first start out in the form of $10^7 - 10^8 M_\odot$ clumps of gas and newly formed stars. We will first see such pre-galactic clumps when they give off sufficient radiation to be detected, at a lookback time that we call t_f . The Pascarelle et al. (1996) cluster of 18 subgalactic sized objects at $z \simeq 2.4$ is an example of this process. We stress, however, that in hierarchical CDM models the formation of these clumps does not have to be coeval, and will in fact likely happen over a wide range of epochs ($z \simeq 1-4$). When these clumps start to combine and form ever larger clumps, at a smaller lookback time $t_m (< t_f)$, we will begin to see the merged clumps as galaxies of morphologies that are familiar to us today: E/S0's, Sabc's, Sd/ Irr's.

At lookback times smaller than t_m (i.e., after the merging epoch began), hierarchical models predict that we will see galaxies with a range of morphological types not dissimilar to what we see today, but with a galaxy mix that is not necessarily equal to the local one. What we will *not* know — if hierarchical clustering is correct — is what a particular galaxy at a lookback time smaller than t_m will look like today. Will it simply passively evolve? Or will it merge with its nearest neighbors, turning (temporarily) into another type of galaxy altogether? In other words, in a hierarchical merging scenario, while the galaxy population mix may not change in a statistical manner for lookback times less than t_m , one cannot necessarily uniquely assign galaxy of type X at high redshift with galaxy of type X today.

The lack of change in the distribution of edge-on systems with ellipticity that we observe is consistent with hierarchical clustering in the following sense. We know from the distribution of Hubble types today that bulge-dominated galaxies comprise the minority of giant galaxies (less than 30%, see Dressler 1980). If all galaxies initially are formed as disk-type systems, with subsequent merging producing pronounced spiral bulges and E/S0 galaxies, then we would expect a steady migration from galaxies with low b/a to those with high b/a . While such a trend is suggested in the present comparison, the observed result is barely of one-sigma significance. The problem is observational: It is difficult to accurately measure the ellipticities of galaxies with $b/a > 0.85$. Errors in photometry will always scatter ellipticities away from $b/a = 1.0$ (since b/a cannot be larger than 1), always depopulating the highest bin in $f(b/a)$. As discussed in the introduction and in §3.2, our systematic correction of the RC3 axis ratios, as well as uncertainties related to the triaxiality of early-type galaxies, makes treatment of the high b/a systems problematic.

If there is one place in comparing the ellipticity distributions of nearby and distant galaxies to hide evolutionary effects, it is among galaxies with $b/a \geq 0.85$. Yet, this is where many merger products are likely to end up in terms of their intrinsic axial ratios. What we conclude is that nature apparently conspires to have systematic effects (observational ones and those due to the redshift) on the ellipticity distributions to essentially cancel the effects expected from the evolutionary change in galaxy morphology. If the hierarchical clustering/merging picture is correct, then the kind of ellipticity test that we have done in this paper is in essence a null test. If we had seen a difference at high ellipticities, it would have been a surprising result. By seeing none, we are consistent with the standard hierarchical clustering/merger model.

We believe that there is enough evidence now to give a reasonable estimate to the redshift corresponding to a lookback time of t_m . Pascarelle et al. (1996) have shown that at least in one direction at $z=2.39$, we still find the subclumps that have generally not yet merged into morphologies recognizable today. If we make the reasonable estimate that

the high redshift galaxies in our ellipticity sample are outnumbered by those at $z \lesssim 1$ (see Figure 2 of Sawicki et al. 1997), we conclude that whatever changes in morphology that have occurred since $z \leq 1$ must have preferentially occurred among round-appearing galaxies - i.e., E, S0 and bulge-dominated spirals. Mergers of systems we would recognize today as galaxies classifiable by the Hubble scheme have therefore been taking place at least as far back as $z \simeq 1$, but likely no farther back than $z \simeq 2.4$. This would argue that $1.0 \lesssim z_{t_m} \lesssim 2.5$, with the most likely time being $1.5 \lesssim z_{t_m} \lesssim 2.0$, consistent with the peak in the star-formation rate in the universe (Madau et al. 1996).

If this view of hierarchical clustering is correct, then understanding how galaxies evolve with time will not be a simple matter of estimating galaxy morphologies and colors at all lookback times. Rather, if what we see at lookback times smaller than t_m , including the present-day, is the current state of mergers, we will need more detailed information about how groupings of galaxies change with time. That information can only come with measurements of redshifts of very faint galaxies, which is a major challenge that the new generation of 8–10 meter telescopes face if we are to truly understand galaxy evolution.

We acknowledge support from HST grants GO.5308.01.93A, GO.5985.01.94A, GO.2684.03.94A, and AR.6385.01.95A. SCO wishes to acknowledge a very useful conversation with R. Blandford and D. Hogg.

REFERENCES

- Abraham, R., Tanvir, N.R., Santiago, B., Ellis, R. S., Glazebrook, K. G. & van den Bergh, S., 1996, MNRAS, 279, L47
- Bertin, E., & Arnouts, K., 1996, in preparation
- Bohlin, R. C., et al. 1991, ApJ, 368, 12
- Brainerd, T., Blandford, R. D., & Smail, I. 1996, ApJ, 466, 623

- Binney, J., & de Vaucouleurs, G. 1980, MNRAS, 194, 679
- Burg, C., Windhorst, R., Odewahn, S., de Jong, R., & Frogel, J. 1997 in Proceedings of the Maryland Workshop on “The Ultraviolet Universe at Low and High Redshift: Probing the Progress of Galaxy Evolution”, Eds. M. Fanelli, & W. Waller, AIP Conf. Ser., in press
- Cowie, L. L., Songaila, A., Hu, E. M., & Cohen, J. G. 1996, AJ, 112, 839
- Dalcanton, J., & Sheckman, S. A., 1996, ApJ, 465, L9
- de Vaucouleurs, G., de Vaucouleurs, A., Corwin, H.G., Buta, R., Paturel, G. & Fougu  , P. 1991, The Third Reference Catalog of Bright Galaxies, Springer Verlag: New York, (RC3)
- de Vaucouleurs, G. & Pence 1973, BAAS, 5, 466
- de Vaucouleurs, G. 1959, *Handbuch der Physik*, 53, 311
- de Jong, R. S., & van der Kruit, P. C. 1994, A&AS, 106, 451.
- Dressler, A. 1980, ApJ, 236, 351
- Driver, S. P., Windhorst, R. A., Ostrander, E. J., Keel, W. C., Griffiths, R. E. & Ratnatunga, K. U. 1995a, ApJ, 449, L23 (D95a)
- Driver, S. P., Windhorst, R. A., & Griffiths, R. E. 1995b, ApJ, 453, 48 (D95b)
- Ellis, R., Colless, M., Broadhurst, M., Heyl, J., & Glazebrook, K. 1996, MNRAS, 280, 235
- Fasano, G. & Vio, R. 1991, MNRAS, 249, 629
- Ferguson, H.C. & Sandage, A. 1989, ApJ, 346, L53
- Frei, Z. et al. 1996, AJ, 111, 174

- Giavalisco, M., Livio, M., Bohlin, R., Macchetto, D. F., & Stecher, T. P. 1996, *AJ*, 112, 364
- Glazebrook, K., Ellis, R. E. Santiago, B., & Griffiths, R. E. 1995, *MNRAS*, 275, L19
- Gott, J. R., & Rees, M. R. 1975, *A&A* 15, 235
- Hill, J. K. et al. 1992, *ApJ*, 395, L37
- Holtzman, J. A., et al. 1995, *PASP*, 107, 1065
- Hubble, E. 1926, *ApJ*, 64, 321
- Huchra, J., Geller, M., De Lapparent, V., & Burg, R., 1988, *IAU Symposium* 130, Large-Scale Structures of the Universe, ed. J. Audouze, M. Pelletto, and A. Szalay, Kluwer, 105
- Im, M. et al. 1995, *ApJ*, 445, L15
- Kaiser, N. & Squires, G. 1993, *ApJ*, 404, 441
- Lambas, D. G., Maddox, S.J., & Loveday, J. 1992, *MNRAS*, 258, 404
- Lilly, S. J., Tresse, L., Hammer, F., Crampton, D., & LeFevre, O. 1995, *ApJ*, 455, 108
- Madau, P. et al. 1996, *MNRAS*, 283, 1388
- Marcum, P. et al. 1997 in *Proceedings of the Maryland Workshop on “The Ultraviolet Universe at Low and High Redshift: Probing the Progress of Galaxy Evolution”*, Eds. M. Fanelli, & W. Waller, *AIP Conf. Ser.*, in press
- Mould, J., Blandford, R., Villumsen, J., Brainerd, T., Smail, I., Small, T., & Kells, W. 1994, *MNRAS*, 271, 31
- Mutz, S. B., et al. 1994, *ApJ*, 434, L55
- Noerdlinger, A. 1979, *ApJ*, 234, 802

- O’Connell, R. et al. 1997 in Proceedings of the Maryland Workshop on “The Ultraviolet Universe at Low and High Redshift: Probing the Progress of Galaxy Evolution”, Eds. M. Fanelli, & W. Waller, AIP Conf. Ser., in press
- Odewahn, S.C. 1997, Nonlinear Signal and Image Analysis, Annals of the New York Academy of Sciences, 188, 184
- Odewahn, S.C., Windhorst, R. A., Driver, S. P., & Keel, W. C. 1996, ApJ, 472, L13
- Odewahn, S. C, & Aldering, G. 1995, AJ, 110, 2009
- Odewahn, S. C. 1995, PASP, 107, 770
- Odewahn, S.C. 1989, Ph.D. thesis, Univ. of Texas
- Pascarelle, S. M., Windhorst, R. A., Keel, W. C., & Odewahn, S. C. 1996, Nature, 383, 45
- Peebles, P. J. E. 1993, “Principles of Physical Cosmology”, (Princeton University Press), Princeton, New Jersey
- Press, W. H., Flannery, B. P., Teukolsky, S. A., and Vetterling, W. T. 1986, Numerical Recipes, (Cambridge University Press), 472
- Ryden, B. S. & Terndrup, D. M. 1994, ApJ, 425, 43
- Sandage, A., Freeman, K. C., & Stokes, N. 1970, ApJ, 160, 831
- Sawicki, M. J., Lin, H., & Yee, H. 1997, AJ, 113, 1
- Smoot, G. F., Bennett, C. L., Kogut, A., & Wright, E. L., 1992, ApJ, 396, L7
- Tyson, J. A. 1985, Nature, 316, 799
- Tyson, J. A., Valdes, F., & Wenk, R. A. 1990, ApJ, 349, L1
- Williams, R.E. et al. 1996, AJ, 112, 1335
- Windhorst, R. A., Keel, W. C., & Pascarelle, S. M. 1997, ApJ, submitted

Windhorst, R. A., Burstein, D., Mathis, D. F., Neuschaefer, L. W., Bertola, F., Buson, L.,
Matthews, K., Barthel, P. D., & Chambers, K. C. 1991, ApJ, 380, 362

Weedman, D. W., 1986, in *Quasar Astronomy* (Cambridge: Cambridge University Press)

Fig. 1.— Using 176 simulated high z images based on observed I_{814} -band WFPC2 images with $I \leq 22$ (and assumed $z \lesssim 0.5$) and intrinsic axis ratio $b/a \leq 0.5$, we plot the residual axis ratio, $(b/a)_o - (b/a)_z$, as a function of signal-to-noise ratio ($\log(S/N)$) in panel a (left) and image resolution $\log(R)$ in panel b (right). Both of these tests predict residuals in the sense expected: faint, low S/N compact images are measured to be systematically too round.

Fig. 2.— Comparison between the eyeball RC3 b/a values derived from $\log R_{25}$ and those derived from the automated MORPHO package. Shown are 63 galaxies observed in B_J by Frei et al. (1996; open circles) and 82 galaxies observed in B_{CCD} by de Jong (1996; open squares). A linear least squares fit to the (eyeball-machine) residuals gives a slope of 0.21 ± 0.01 and an r.m.s. scatter about the best fit (dashed) line of 0.07. The fit was made only with the Frei data which cover an adequate range in b/a , but the de Jong sample (by selection has $b/a \geq 0.6$), were plotted to show consistency with the derived fit. Based on this fit, we adopted the correction formula in the text (equation 5) to transform the 1569 RC3 (eyeball) axis ratios to the system defined by the MORPHO automated ellipse fitting software used to reduce all our WFPC2 faint galaxy images.

Fig. 3.— The differential frequency distributions of apparent axis ratio, b/a , for four I_{814} -band ranges are plotted using open circles connected by thin dashed lines. The *local* RC3 galaxy b/a distribution is plotted in each panel using filled squares connected by bold lines. The RC3 data were redshifted assuming $H_0 = 75$ km/sec/Mpc, $q_0 = 0.5$, plus K-corrections and luminosity evolution estimates discussed in the text. No systematic corrections for R or S/N effects have been applied to the RC3 data in this figure.

Fig. 4.— As in Figure 3, but systematic corrections for Resolution effects have been applied to the RC3 b/a estimates. No statistically significant difference is seen between the RC3 sample moved out to high redshift and the observed WFPC2 I_{814} -band samples, even for galaxies with low b/a values.

Fig. 5.— As in Figure 3, but the local Type fractions in the RC3 for E+S0, Sabc, and Sd+Irr galaxies have been altered from 32%, 48%, and 18%, respectively, to a spiral-rich sample of 10%, 30%, and 60% at $z \simeq 1$. Systematic corrections for R effects have been applied to the RC3 b/a estimates, as discussed in the text. Note that with these corrections, the higher and lower redshift samples are virtually indistinguishable for $I \gtrsim 22$ mag ($z \gtrsim 0.5$).

Fig. 6.— A montage of galaxies with $0.0 \leq b/a \leq 0.4$ selected at random from the ground-based and HST galaxy samples used in this work. The top row consists of 8 galaxies (observed in B_J) by Frei et al. 1996, and the second shows the appearance of these same galaxies at $z=0.6$, as modeled by MORPHO. In the first row, images are shown at ground-based resolution with each postage stamp image having a linear size of $167''$. In all remaining rows, a WFPC2 resolution ($0.0996''/\text{pix}$) is used with each stamp having a linear dimension of $6.2''$. The remaining 4 rows consist of WFPC2 images in I_{814} roughly corresponding to the four magnitude ranges constituting our faint samples: $14 \leq I_{814} \leq 20$, $20 \leq I_{814} \leq 22$, $22 \leq I_{814} \leq 24$, $24 \leq I_{814} \leq 25$. Each image is normalized to a linear grey-scale from -3σ to $+20\sigma$, where σ is the noise measured in the local background. Morphological features such as spiral arms or strong dust lanes are not prominently seen in the $z \geq 0.4$ rows of WFPC2 images, although such features are still clearly visible in the B_J images modeled for $z = 0.6$. The high redshift systems ($z \geq 0.8$) do appear to display a higher degree of image asymmetry along the major axis and more clumpiness relative to the lower redshift systems.

Fig. 7.— As in Figure 6, but for galaxies with $0.6 \leq b/a \leq 0.75$. As in the $b/a \leq 0.4$ cases of Figure 6, it appears that prominent spiral arms are not seen in the $z \geq 0.8$ rows of WFPC2 images, and the degree of image clumpiness and asymmetry is higher compared to their low redshift counterparts.

Fig. 8.— As in Figure 6, but for galaxies with $0.8 \leq b/a \leq 1.0$. Again no prominent spiral structure is visible for $z \geq 0.8$, but now the impression of increased global image asymmetry is not as strong for the rounder galaxies.

Table 1. WFPC2 Fields Analyzed in F814W

Name	RA (2000) DEC	l,b	A_B	T(sec)	N_{images}
HDF	12:36:49.59 +62:12:54.0	125.9 +54.8	0.00	123600	49
53W002	17:14:15.47 +50:15:28.3	77.0 +35.8	0.03	1700	17
HFF_OW	12:36:21.16 +62:14:27.2	126.0 +54.8	0.00	2500	3
HFF_SW	12:36:33.91 +62:10:54.2	125.9 +54.9	0.00	2500	3
HFF_JW	12:36:35.77 +62:13:40.9	125.9 +54.8	0.00	5300	4
HFF_SE	12:36:47.77 +62:10:19.3	125.9 +54.9	0.00	2500	3
HFF_NW	12:36:50.81 +62:15:41.9	125.9 +54.8	0.00	2500	3
HFF_JE	12:37:03.86 +62:12:15.2	125.8 +54.8	0.00	5300	4
HFF_NE	12:37:05.85 +62:15:06.7	125.8 +54.8	0.00	2500	3
HFF_OE	12:37:17.92 +62:11:33.4	125.8 +54.9	0.00	3000	3
DWG_UEH0	00:53:23.57 +12:33:50.3	123.7 -50.3	0.18	2100	3
DWG_UIM0	03:55:31.91 +09:43:38.5	179.8 -32.1	0.46	866	6
DWG_UOP0	07:50:47.39 +14:40:42.7	206.1 +19.6	0.06	2100	2
DWG_UY40	14:34:48.54 +25:08:11.1	033.9 +66.8	0.04	1000	6
DWG_UX40	15:19:41.22 +23:52:04.3	035.8 +56.5	0.14	1875	4
DWG_USA2	17:12:23.17 +33:35:48.5	056.7 +34.3	0.12	2100	3

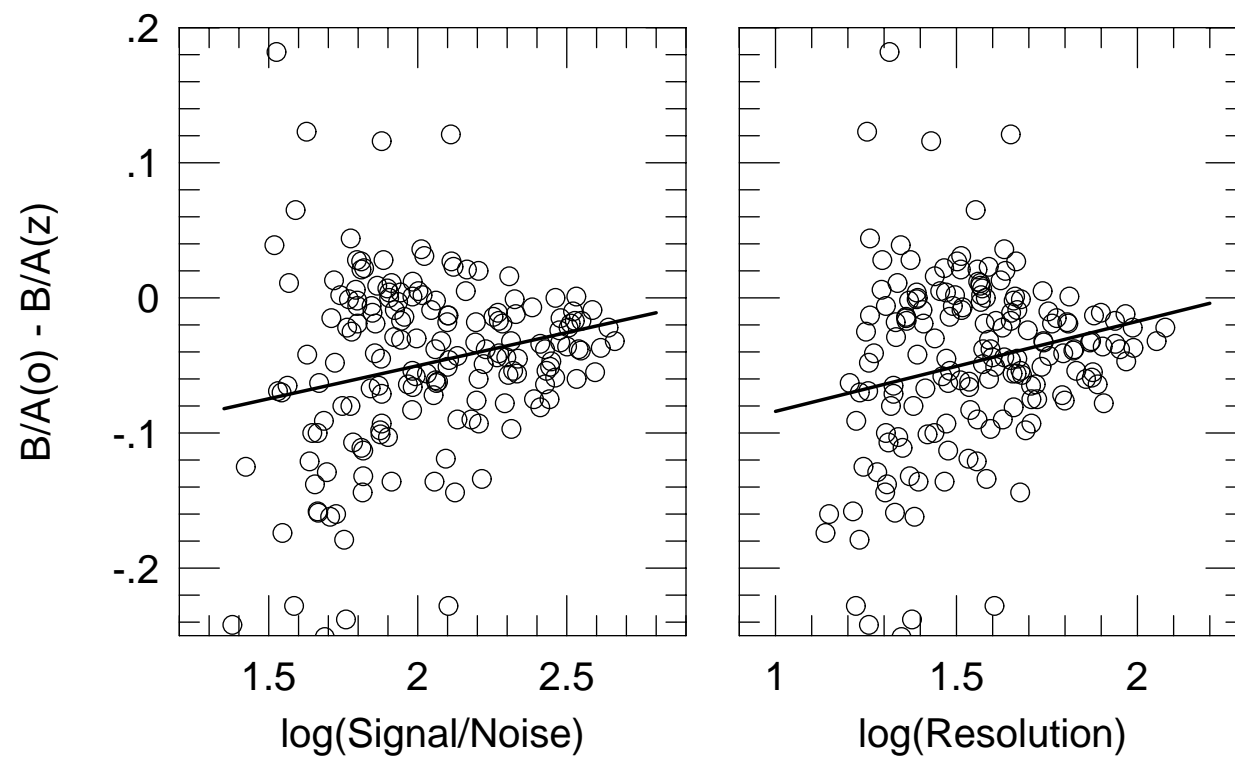


Fig. 1

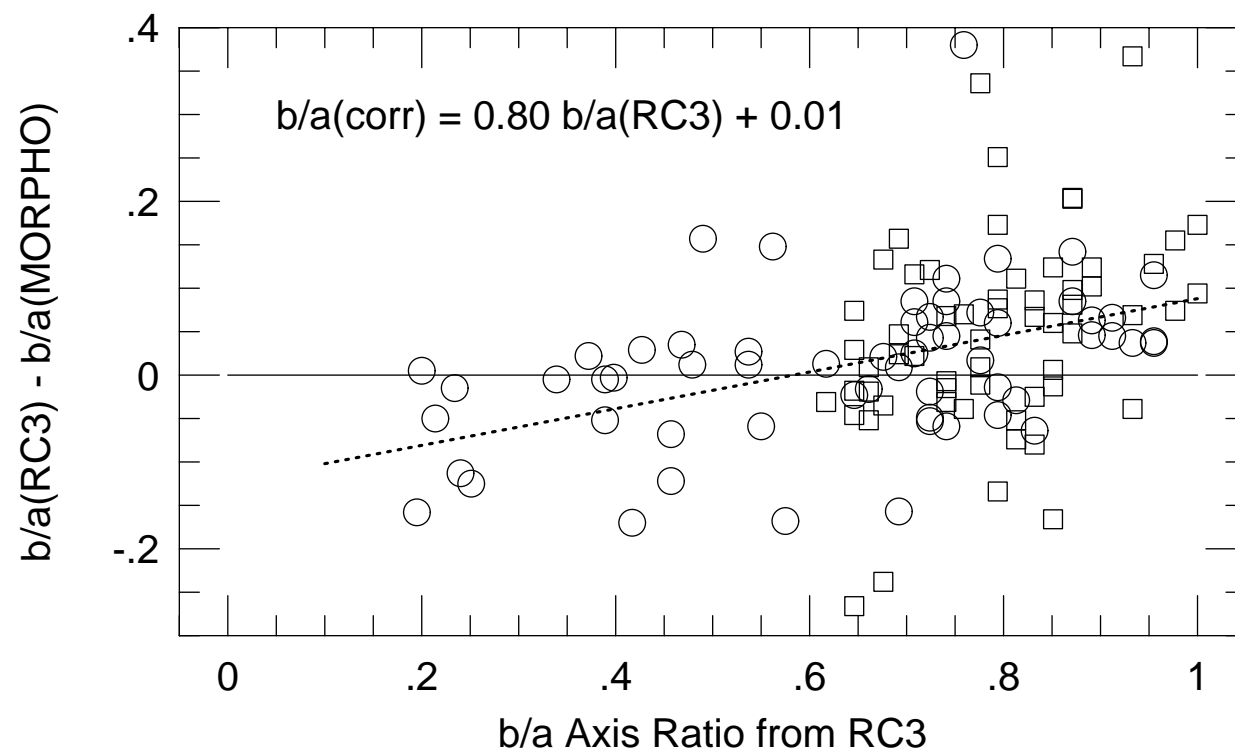


Fig. 2

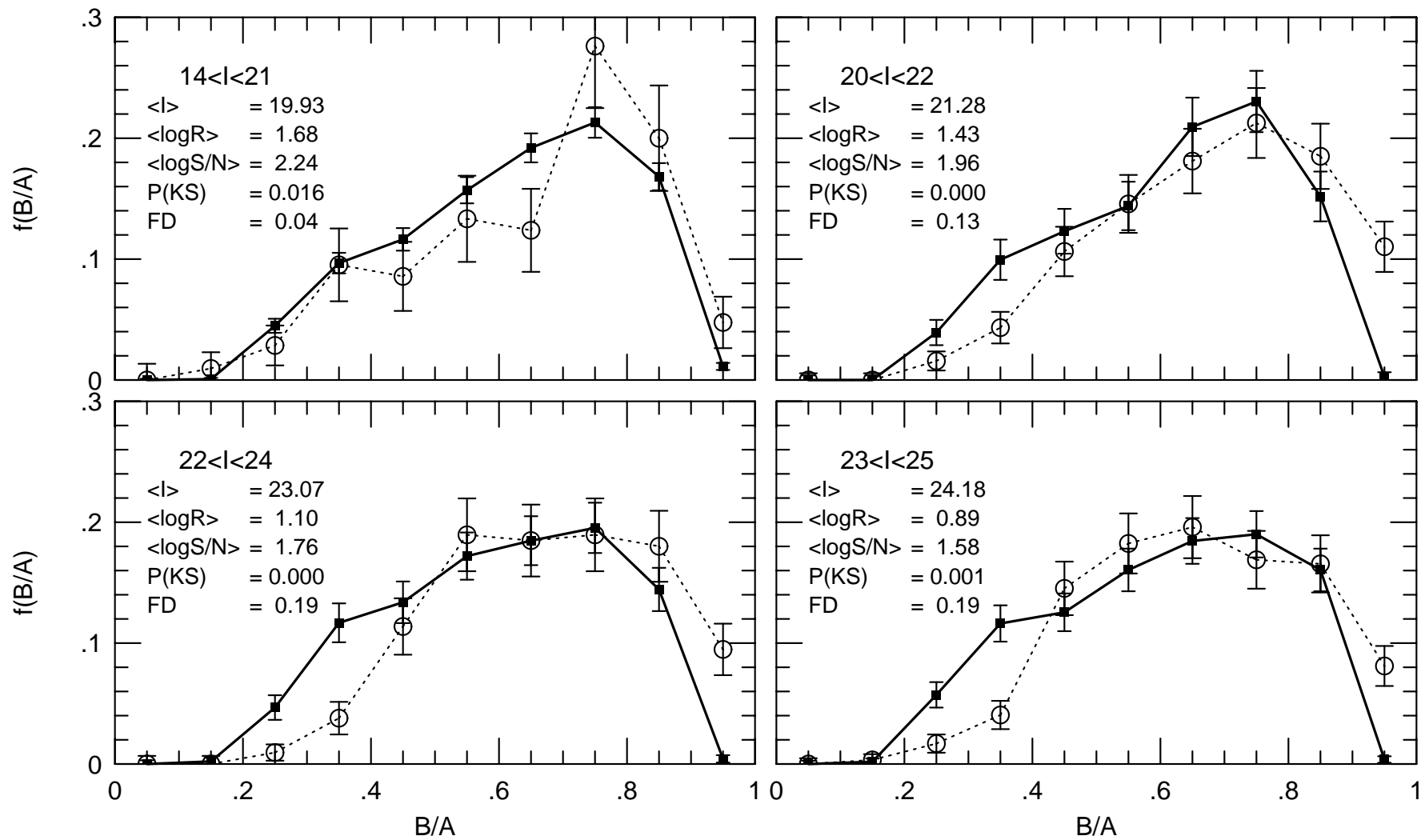


Fig. 3

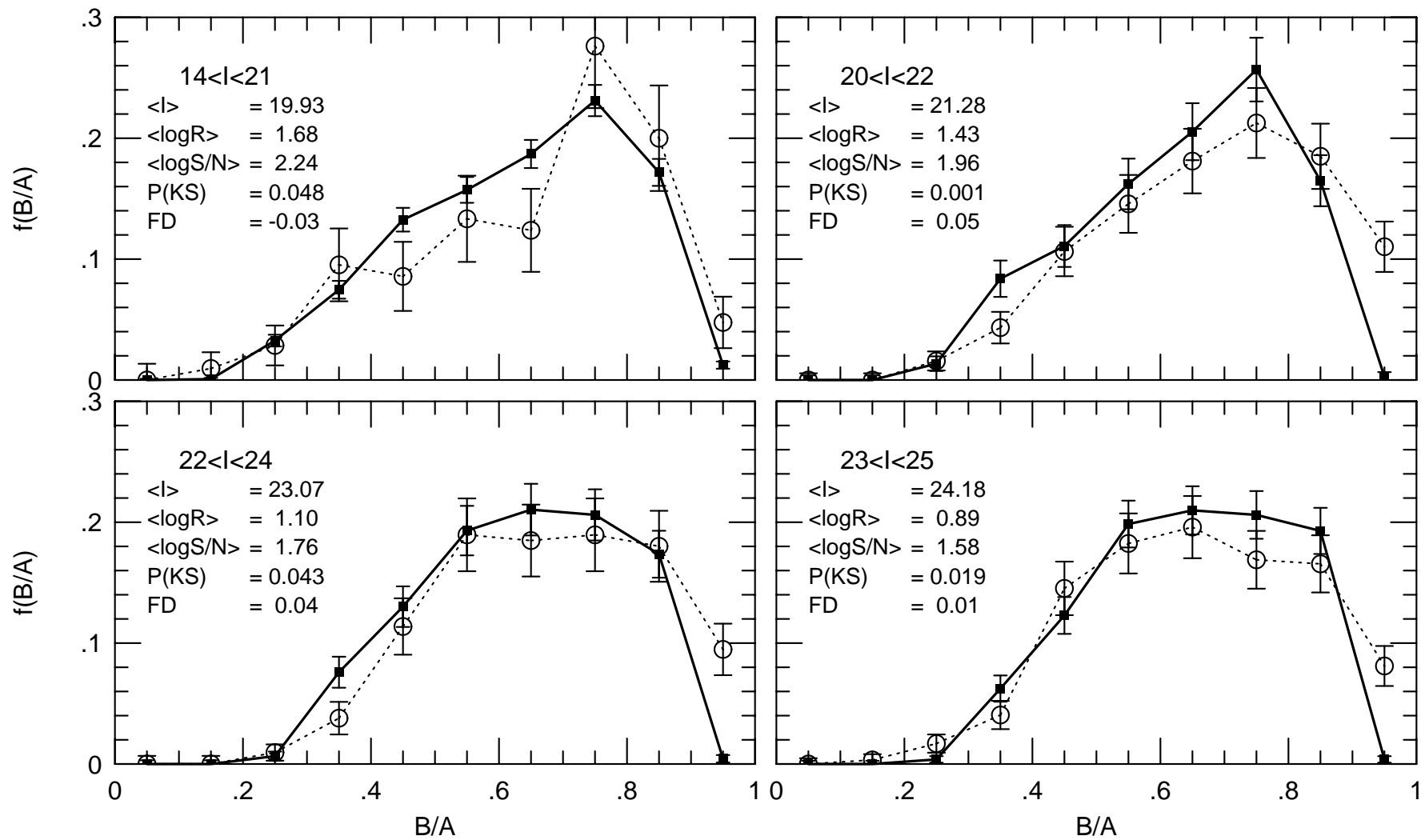


Fig. 4

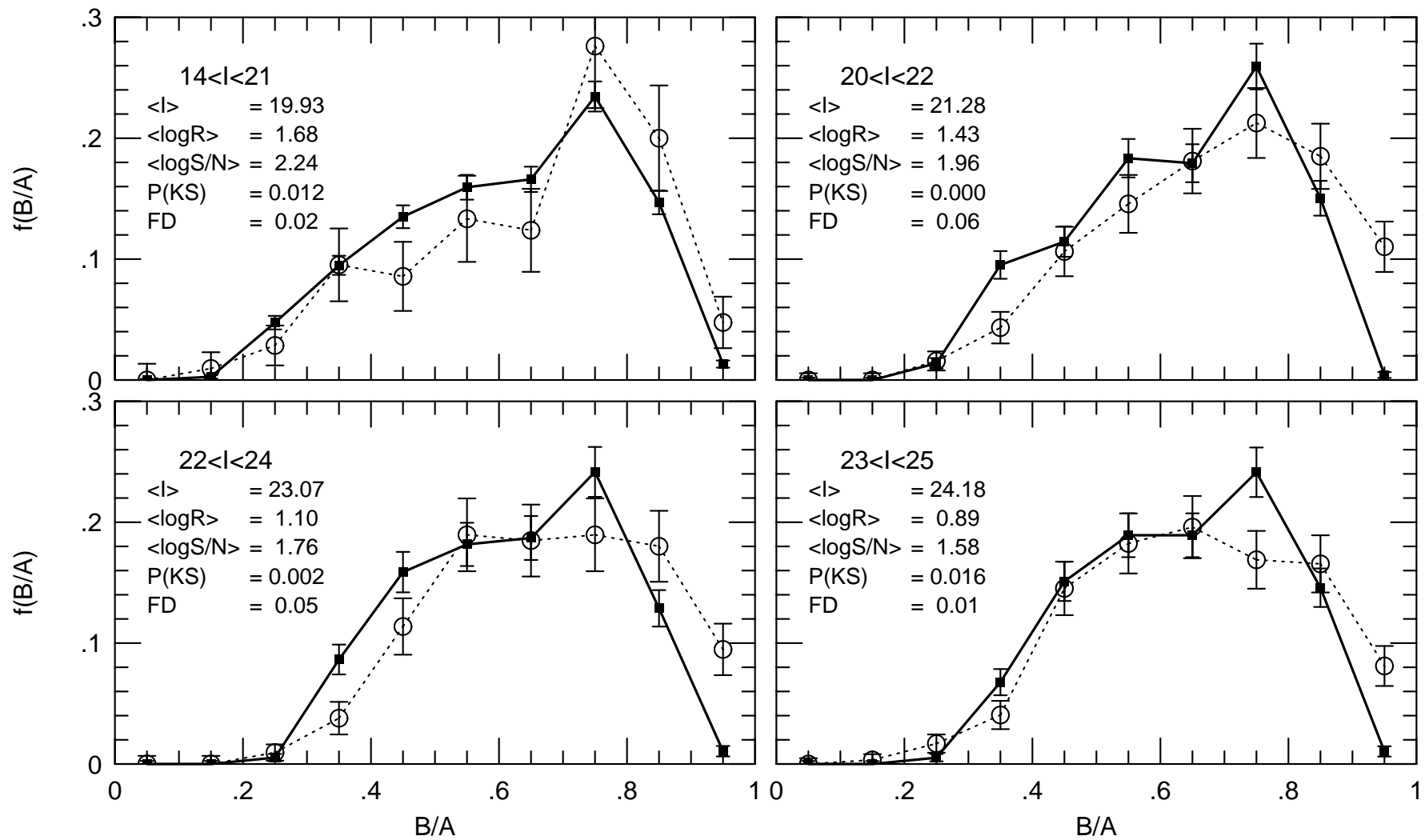
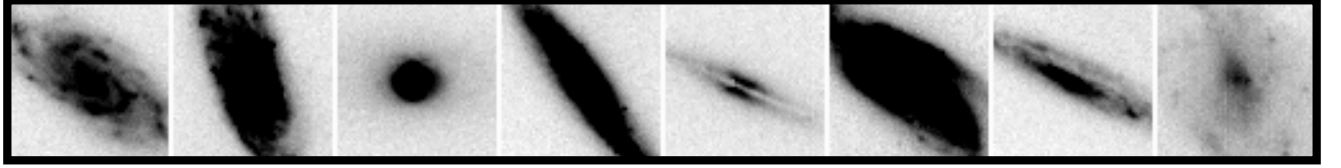
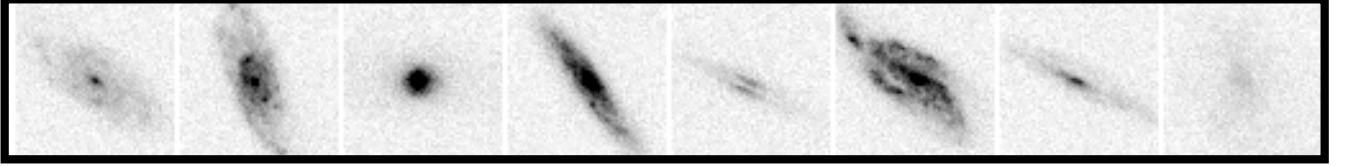


Fig. 5

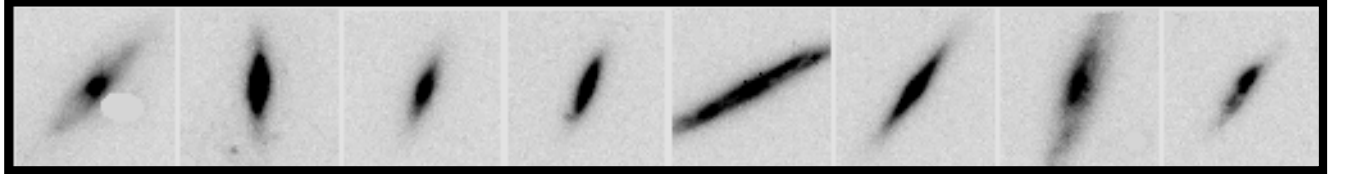
Frei Bj $z \sim 0.007$



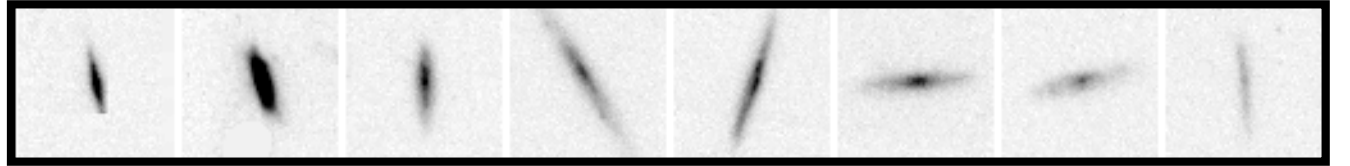
Frei Bj $z \sim 0.6$



$14 < I(F814W) < 20$ $z \sim 0.1$



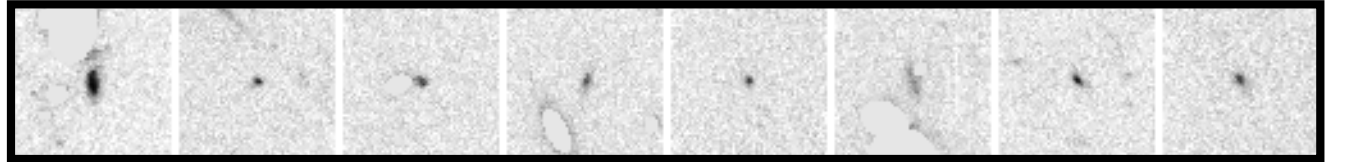
$20 < I(F814W) < 22$ $z \sim 0.4$



$22 < I(F814W) < 24$ $z \sim 0.8$

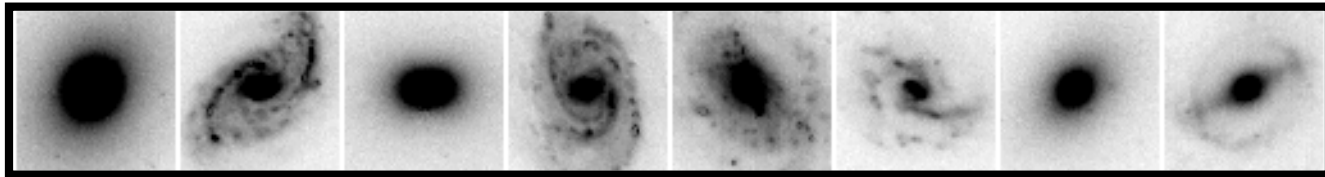


$24 < I(F814W) < 25$ $z \sim 1.1$

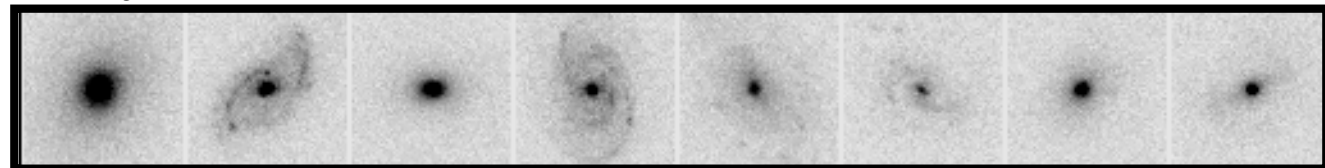


Galaxies with $0.0 < B/A < 0.4$

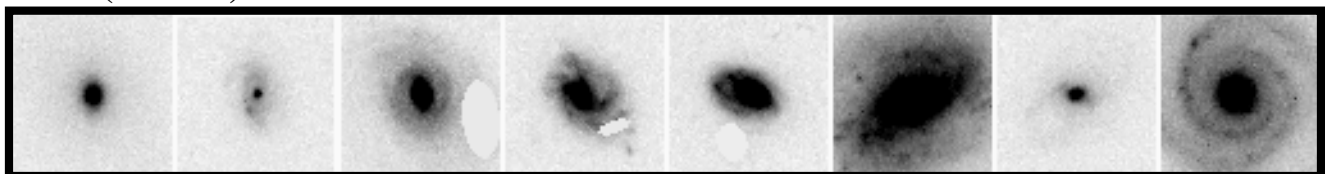
Frei Bj $z \sim 0.007$



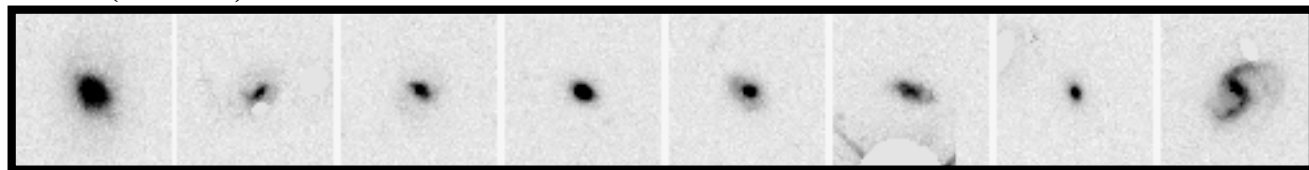
Frei Bj $z \sim 0.6$



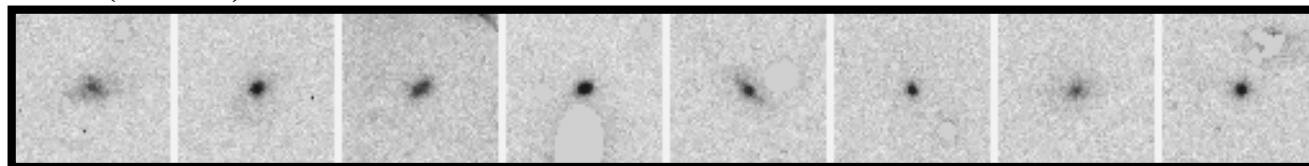
$14 < I(F814W) < 20$ $z \sim 0.1$



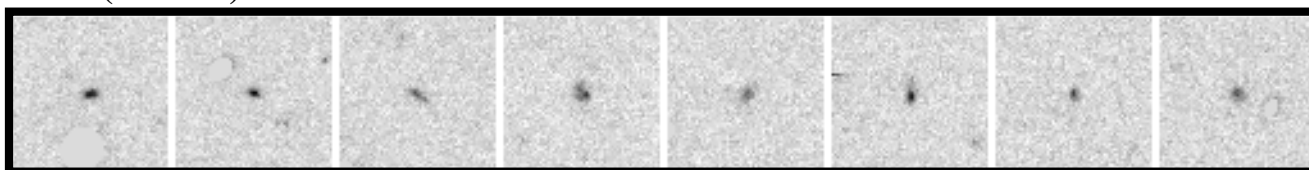
$20 < I(F814W) < 22$ $z \sim 0.4$



$22 < I(F814W) < 24$ $z \sim 0.8$

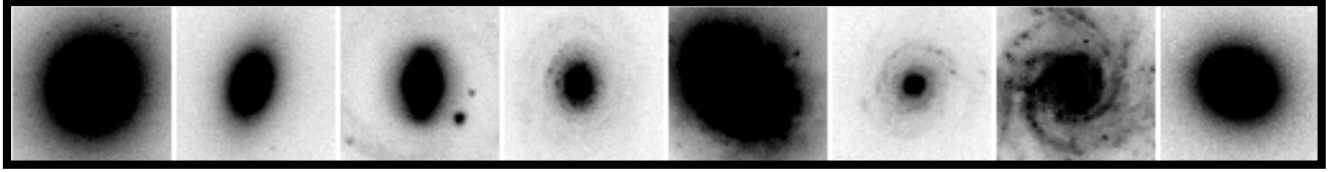


$24 < I(F814W) < 25$ $z \sim 1.1$

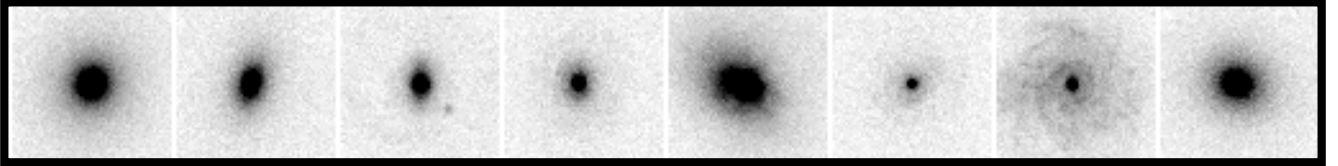


Galaxies with $0.6 < B/A < 0.75$

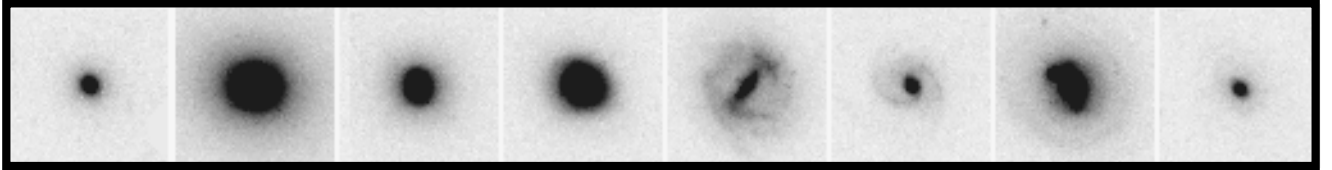
Frei Bj $z \sim 0.007$



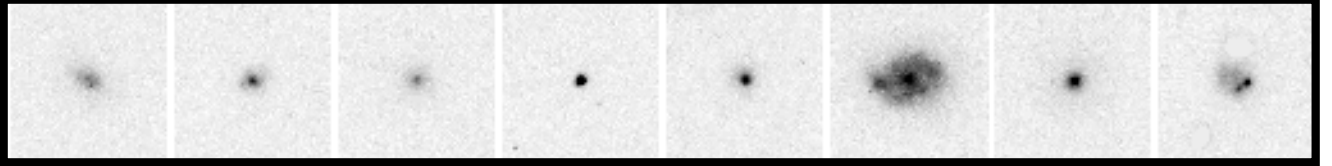
Frei Bj $z \sim 0.6$



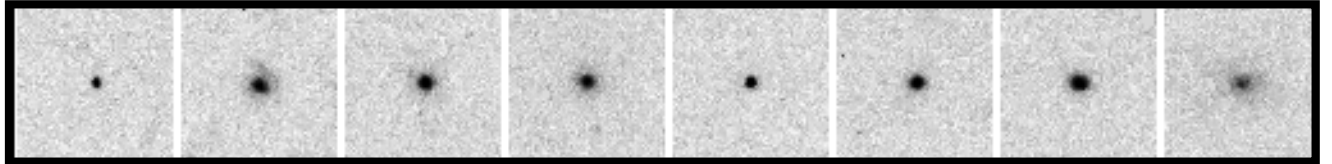
$14 < I(F814W) < 20$ $z \sim 0.1$



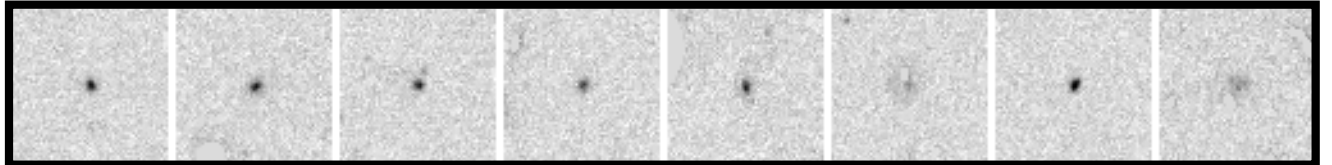
$22 < I(F814W) < 20$ $z \sim 0.4$



$22 < I(F814W) < 24$ $z \sim 0.8$



$24 < I(F814W) < 25$ $z \sim 1.1$



Galaxies with $0.8 < B/A < 1.0$